Mobility Matters at Nanoscale: Rendering the Received Terahertz Signal Power in Human Blood Vessels

Jorge Torres Gómez*, Jennifer Simonjan†, Johan Engstrand‡, Sergi Abadal§, Robin Augustine‡, Thiemo Voigt‡, and Falko Dressler*

* School for Electrical Engineering and Computer Science, TU Berlin, Berlin, Germany

† Technology Innovation Institute, Masdar City, Abu Dhabi, UAE

‡ Department of Electrical Engineering, Uppsala University, Sweden

§ Universitat Politècnica de Catalunya, UPC, Spain

Email: {torres-gomez, dressler}@ccs-labs.org, jennifer.simonjan@tii.ae, abadal@ac.upc.edu, {johan.engstrand, robin.augustine, thiemo.voigt}@angstrom.uu.se

***Abstract*—We evaluate the received power level of transmitted signals between flow-guided nanosensors in human blood vessels. The power budget calculation accounts for the radiation pattern of a dipole-like nanoantenna and the variability of the nanosensor position. We model the nanosensor mobility component not only as displacement but also as the rotation produced by the blood flow. Our results show that the varying distance among nanosensors influences the average power component, while the power level variance results from the antenna's rotation. This simulation model contributes to portraying communication capabilities at the nanoscale, and considering realistic evaluations with the blood flow dynamics.**

***Index Terms*—Internet of Bio-Nano-Things, Terahertz Communications, Nanoantenna, Human Blood Vessels, Mobility**

I. Introduction

Following the vision of internet of bio-nano-things (IoBNT) networks for biomedical applications, nanodevices equipped with communication modules will enable intra-body links [1]. In this endeavor, nanoantennas in the micrometer scale entail graphene-based radiators to operate in the terahertz (THz) band, leveraging the plasmonic properties of graphene [2]. Since the first nanopatch design by Jornet and Akyildiz [3], follow-up designs include dipole-like [4], [5], patches [6], [7] and spiral geometries [8] attaining communication links in the nanoscale.

In practice, operating these nanoantennas for in-body scenarios makes the communication link analysis more challenging. On the one hand, the surrounding tissue modifies the antenna's radiation pattern; see [9, Fig. 6]. On the other hand, its orientation can not be predefined in advance in real-world applications as the nanosensor flows passively with the blood. Although there is reported research on the use of nanoantennas in human vessels, see [10], describing a realistic use case for communications is still an open research direction.

This paper provides a model to derive the time-varying received power, focusing on a communication link between nanosensors traveling in human blood vessels. We evaluate the power budget while including the gain of the dipole-like nanoantenna and following the design in [4], [5]. When modeling the gain, the nanoantenna was surrounded by blood and isolated with a spherical cover made of polydimethylsiloxane (PDMS), as illustrated in Fig. 1. We model the mobility component with the nanosensors' displacement and the antenna rotation that the flow impinges on. This setup provides means to characterize and evaluate the received power with the dynamics of the blood fluid in realistic cases.

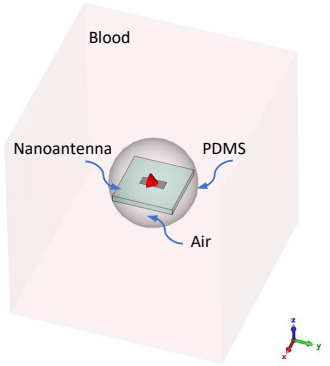

Fig. 1. The antenna is modeled in CST as being shielded within a sphere made of biocompatible PDMS material,surrounded by blood.

Aiming to describe the received signal power, our key contributions can be summarized as follows:

- We provide a realistic simulation model to evaluate received signal power levels of nanosensors guided by the blood flow,[1] and
- we provide insights on the probabilistic description of the received power with time.

Following these two contributions, we structure this paper as follows: The nanoantenna design and simulation are described

[1]We provide open access to the CST nanoantenna model and the mobility model at https://github.com/jorge-torresgomez/terahertz_inbody.

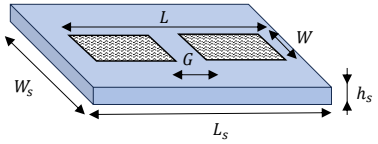

Fig. 2. A schematic representation of the nanoantenna [4], [11].

in Section II. This section provides realistic figures for the antenna's radiation pattern and includes the blood's modeling as a dielectric medium. Next, we analyze in Section III the mobility model of nanosensors flowing in the human vessels, including displacement and rotation. We formulate the received power at a nanosensor encompassing the variability of the antennas' gain in the line of sight (LoS) direction between the emitter and the receiver and the path loss attenuation in blood. Finally, we illustrate results for the receiver power with time in Section IV. We also numerically evaluate the corresponding Probability Density Function (PDF) of the received power. Looking at its random nature, we provide insights into its average and variability.

II. Graphene-based Nanoantenna

We base our design on a previously reported dipole antenna by Tamagnone et al. [4], also reported in [5]. This antenna design consists of two graphene patches on a quartz substrate, as Fig. 2 illustrates. The antenna is modeled in CST Studio Suite 2021 by assembling three bricks, which account for the substrate and the two patches. We excite the antenna through a discrete port that connects the two graphene patches. The port impedance equals the input antenna impedance Z_0 as measured with the simulator.

A brick made of lossless quartz with a permittivity of $3.75\,\mathrm{F/m}$ models the antenna substrate. The brick has dimensions $L_\mathrm{s} \times W_\mathrm{s} \times h_\mathrm{s}$, as shown in Fig. 2, with the values listed in Table I. The two graphene patches are also built with two bricks of zero height, the same width W and total length L, and a vacuum gap of length G in between. The two patches are centered on the upper side face of the substrate as depicted in Fig. 2. We added graphene to CST by defining a new material with the relaxation time and chemical potential listed in Table I.[2]

The antenna is wrapped in a cover made of PDMS to isolate it from blood.[3] The cover is modeled as a sphere, with the smallest inner radius needed to cover the substrate material (around $37.5\,\mu\mathrm{m}$), and thickness in the micrometer range, also listed in Table I. The inside of the sphere is filled with air. Lastly, we surround the shielded antenna with blood to model the impact of the body. The blood is simulated with a brick of side-length five times the shield's radius; see Fig. 1. The blood material is modeled by its permittivity in the 1 to $4\,\mathrm{THz}$ range. The relative permittivity of blood is calculated as [13, Eq. (11)]

$$\epsilon_\mathrm{r} = \epsilon_\infty + \sum_{p=1}^{2} \frac{\Delta\epsilon_p}{1 + j\omega\tau_p}, \tag{1}$$

where ϵ_∞ is the permittivity at the high frequency limit, $\Delta\epsilon_p$ is an intermediate value for a given relaxation time τ_p, and $\omega = 2\pi f$ is the angular frequency. The values for the parameters are reported in Table II.[4]

[2]The steps to add graphene as a material in CST are demonstrated in this video https://www.youtube.com/watch?v=SeGy_ZhZzEs.

[3]Polydimethylsiloxane (PDMS) is a bio-compatible material typically used for implanted antennas [12].

TABLE I
Antenna parameters.

Parameter	Description	Value
f_c	Operating frequency	$2.107\,\mathrm{THz}$
L	Graphene length	$8.5\,\mu\mathrm{m}$
W	Graphene width	$8\,\mu\mathrm{m}$
h	Graphene thickness	0
E_F	Graphene chemical potential	$0.6\,\mathrm{ps}$
τ	Graphene relaxation time	$1\,\mathrm{ps}$
L_s	Substrate length	$50\,\mu\mathrm{m}$
W_s	Substrate width	$50\,\mu\mathrm{m}$
h_s	Substrate thickness	$5\,\mu\mathrm{m}$
	Quartz permittivity	$3.75\,\mathrm{F\,m}$
$Z_{1,1}$	Antenna input impedance	$324\,\Omega$
r	Shield inner radius[a]	$\approx 35.7\,\mu\mathrm{m}$
	Shield thickness	$0.1\,\mu\mathrm{m}$
	PDMS permittivity	$2.76\,\mathrm{F/m}$

[a]The inner radius of the shield is evaluated as $r^2 = \left(\frac{W_\mathrm{s}}{2}\right)^2 + \left(\frac{L_\mathrm{s}}{2}\right)^2 + h_\mathrm{s}^2$.

TABLE II
Permittivity and relaxation time values in blood [13].

Parameter	ϵ_∞	$\Delta\epsilon_1$	$\Delta\epsilon_2$	τ_1 [ps]	τ_2 [ns]
Value	2.1	130	3.8	14.4	0.1

A. Nanoantenna simulation

The nanoantenna design resonates at $f_\mathrm{c} = 2.107\,\mathrm{THz}$, as results from the simulation. A minimum of approximately $-33\,\mathrm{dB}$ for S_{11} is achieved when the source impedance equals the antenna impedance (where $\mathrm{Im}\{Z_0 = 0\}$). The resulting radiation pattern is illustrated in Fig. 3. The radiation pattern exhibits a maximum antenna gain of approximately $-12\,\mathrm{dBi}$ at the elevation angles $45,\ 135,\ 225$ and 315° in the xz-plane. The resulting lobe width span is 35°.

The radiation pattern in Fig. 3 differs from the dipole-like design due to the impact of the surrounding PDMS material and blood. Both materials are in the near field of the radiator, as the radius of the cover shield is less than the Fraunhofer distance; i.e., $r = 35.7\,\mu\mathrm{m} < 2\frac{2L_\mathrm{s}^2}{\lambda} \approx 70\,\mu\mathrm{m}$, where L_s is the length of the substrate, $\lambda = c/f_\mathrm{c}$ is the wavelength, c is the speed of light, and $f_\mathrm{c} = 2.107\,\mathrm{THz}$ the resonator frequency.

[4]The obtained permittivity values are imported in CST by defining a new material and following the steps in this video https://www.youtube.com/watch?v=Fa23oNEeiyg.

As a consequence of this radiation pattern, the nanoantenna radiates the least power in the xy-plane; i.e., $< -90\,\mathrm{dB}$ in the y-direction. The power loss is in the range -60 to $-35\,\mathrm{dB}$ in the surface of the cover shield.

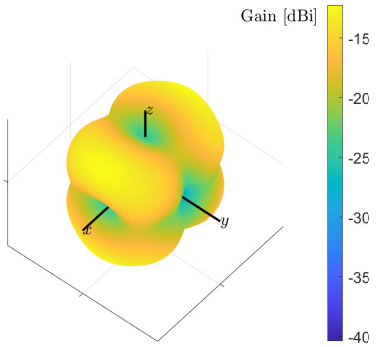

Fig. 3. Radiation pattern of the nanoantenna inserted in blood.

III. Communication Model in the Human Vessels

The mobility of the nanodevice in the blood flow impacts the communication performance due to the effect of displacement and rotation. The nanodevice displacement increases or decreases the received power with the varying distance to the receiver node. Besides, the perceived gain changes with time as the nanodevice rotates while displacing. Depending on the antenna orientation with the receiver node, the gain strives maximum (around $-12\,\mathrm{dB}$) or minimum (around $-40\,\mathrm{dB}$); which will also impact the received power.

We describe in this section the communication performance with the received power, as the power level ultimately defines the perceived signal-to-noise ratio (SNR) in the link. The next two subsections model the antenna's mobility with the blood flow and the corresponding power budget.

A. Nanodevice mobility with the blood flow

Two mobility components will impact the power level due to the nanodevice's displacement along the vessel [14] and its rotation caused by the flow. The displacement component is determined by diffusion and advection; diffusion will be produced by the interaction of the nanodevices with the blood components and is described with the diffusion coefficient for a sphere as [15, Eq. (2)]

$$D_n = \frac{k_\mathrm{B} T}{6\pi\eta r} \approx 2\times 10^{-15}\,\frac{\mathrm{m}}{\mathrm{s}^2}, \tag{2}$$

where $k_\mathrm{B} = 1.38\times 10^{-23}\,\mathrm{J/K}$ is the Boltzmann constant, $T = 300\,\mathrm{K}$ is the temperature of the system, $\eta = 3\times 10^{-3}\,\mathrm{kg/(m\,s)}$ is the blood viscosity [16], and $r \approx 35.7\,\mu\mathrm{m}$ is the radius of the sphere, as listed in Table I.

For the advection component, we assume the nanodevice travels at the speed of the blood, denoted as v. Thereby, its position along the y-axis in Fig. 4 will be given by $y = v\Delta t$, and the speed is calculated as [17, Eq. 4.9 pag. 54]

$$v(z) = \frac{v_c}{r_v^2}\left(2r_v(z+r_v) - (z+r_v)^2\right), \quad z\in[-r_v,\, r_v], \tag{3}$$

where z, centered at the vessel center, refers to the z-coordinate of the nanodevice position; see Fig. 4. The variable r_v is the vessel radius and v_c stands for the maximum speed at the vessel center given as

$$v_c = \frac{\Delta P r_v^2}{2\eta l_v}. \tag{4}$$

where ΔP is the pressure difference along the vessel segment, η is the blood viscosity, and l_v is the length of the vessel segment, as represented in Fig. 4.

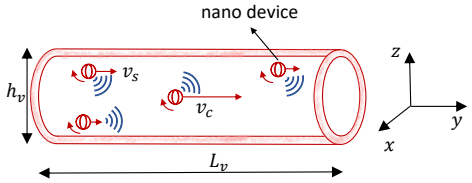

Fig. 4. Mobility and rotation of nanodevices along the vessel segments.

With Equations (2) and (3), we evaluate whether advection dominates diffusion with the Péclet number as [15, Eq. (19)]

$$P_\mathrm{e} = \frac{v(z)\times d}{D_n} \sim 10^6, \tag{5}$$

when considering the center speed in the vessel as $v_c \sim 10^{-3}\mathrm{m/s}$ as in the arterioles, see [18, Table I], the propagation distance $d \sim \mu\mathrm{m}$ and the diffusion coefficient of 10^{-16} orders magnitude, as given in Eq. (2). According to this calculation, the Péclet number is greatly larger than the unit, which means that the nanosensor traveling in the center of the vessel segment follows a straight path (cf. Fig. 4).

Advection also dominates for the nanosensors traveling close to the vessel walls. With the diameter of the arterioles vessel, $\sim 200\,\mu\mathrm{m}$ see [18, Table I], and the nanosensor's size $\sim 35.7\,\mu\mathrm{m}$ see the radius in Table I, we evaluate its closest center's position to the vessel wall and the corresponding speed with Eq. (3). As the corresponding speed is in the order of $10^{-4}\mathrm{m/s}$ when using Eq. (3), the resulting Péclet number yields in the order of 10^7 for the same traveling distance in the $\mu\mathrm{m}$ scale.

B. Rotation of the nanoantenna

In addition to the displacement component, the nanosensor will also rotate due to the impact of the fluid. Following the fluid's direction and the nanosensor's spherical shape, it will experience a clockwise rotation of uniform speed, here denoted as $\dot{\omega}$; see [19, Fig. 7-3.2 pp. 299]. The rotation speed, evaluated through the torque force of magnitude $|\mathbf{T}|$, results notably fast as evaluates

$$\dot{\omega} = \frac{|\mathbf{T}|}{m\, r_\mathrm{Tx}^2} \approx 692\frac{\mathrm{rad}}{\mathrm{ms}}, \tag{6}$$

where the product $m\, r_\mathrm{Tx}^2$ refers to the moment of inertia, $m = m_\mathrm{quartz} + m_\mathrm{PDMS} \approx 10^{-11}\mathrm{kg}$ is the total mass of the transmitter after adding the mass of quartz and PDMS components. The mass of both components is calculated with their corresponding densities and volumes as $\rho \times V$, where $\rho_\mathrm{quartz} = 2.65\times 10^3\,\mathrm{kg/m^3}$ is the density of quartz,

$\rho_{\text{PDMS}} = 0.97 \times 10^3\,\text{kg/m}^3$ is the density of PDMS [20]. The volumes are readily evaluated with the product of height, length, and width for the bricks, and with the shield radius for the spheric volume, as follows from the values listed in Table I.

We calculate the torque vector using the first term in [21, Eq. (7.3.97) pp. 313] (as an accurate approximation of the total torque), yielding

$$\mathbf{T} = -\mathbf{i}_y\, 32\,\pi\,\mu\, r_{\text{Tx}}^3\, v_c\, \frac{\text{Tx}_{\text{posz}}}{h_v^2} \approx -\mathbf{i}_y 3 \times 10^{-14}\text{N m}, \quad (7)$$

where $\text{Tx}_{\text{posz}} \approx 90\,\mu\text{m}$ is the transmitter position from the vessel center, $\mu = 3 \times 10^{-3}\,\text{Pa s}$ denotes the blood viscosity, $v_c = 1 \times 10^{-3}\,\text{m/s}$ is the speed in the vessel center in the arterioles, and $h_v = 200\,\mu\text{m}$ is the vessel thickness (see [18, Table I]). As this equation indicates, the torque force is in the negative direction of the y-axis. Following the right-hand grip rule, this torque produces the spheric nanosensor's clockwise rotation around the x axis. The magnitude of the torque vector is computed considering the nanosensor travels at a distance of $\text{Tx}_{\text{posz}} \approx 90\,\mu\text{m}$ from the vessel center.

The sphere's rotation also produces the rotation of the antenna's radiation pattern. Assuming an initial orientation with the vector $\mathbf{g}_0$ (as the vector normal to the upper plane substrate in Fig. 1), the orientation of the antenna with time can be evaluated with the rotation matrix along the x-axis as

$$\mathbf{g}(t) = \mathbf{A}_x(t)\mathbf{g}_0, \quad (8)$$

where

$$\mathbf{A}_x = \begin{bmatrix} 1 & 0 & 0 \\ 0 & \cos(\omega t) & -\sin(\omega t), \\ 0 & \sin(\omega t) & \cos(\omega t) \end{bmatrix} \quad (9)$$

is the rotation matrix.

C. Power budget in the blood

To determine the received power of the signal, we need to model the communication channel between the sensors in the blood. The received power is expressed as

$$P_{\text{Rx}}(t) = P_{\text{Tx}} + G_{\text{Tx}}(t) + G_{\text{Rx}}(t) - L_v(t)\,[\text{dB}], \quad (10)$$

where P_{Tx} is the transmit power, $L_v(t)$ is the path loss of the signal and $G_{\text{Tx}}(t)$ and $G_{\text{Rx}}(t)$ are the gains of the transmitting and receiving antennas, respectively. The path loss $L_v(t)$, which is mainly determined by the varying distance $d(t)$, is formulated with the spreading and molecular absorption loss (scattering loss is negligible [13]) as

$$L_v(t) = -10\log_{10}\left(e^{-\mu_{\text{abs}}d(t)}\frac{\lambda_{\text{g}}}{(4\pi d(t))^2}\right)\,[\text{dB}], \quad (11)$$

where $\mu_{abs} = 4\pi n''/\lambda_{\text{g}}$ is the molecular absorption coefficient, $d(t)$ is the distance between sender and receiver, and $\lambda_{\text{g}} = \lambda/n'$ is the effective wavelength. The terms n' and n'' are the real and imaginary parts of the refractive index n of the medium the wave is travelling through (blood in our case). More detailed channel and dielectric characteristics of blood can be found in [22], [23].

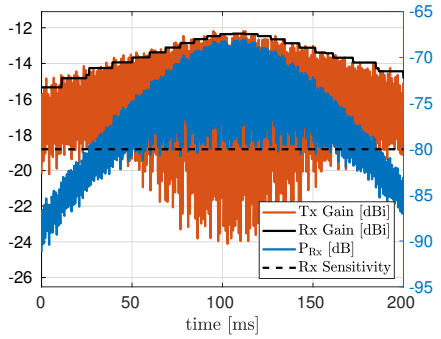

Fig. 5. Received power and antenna gain over time as the nanoantennas flow with the blood.

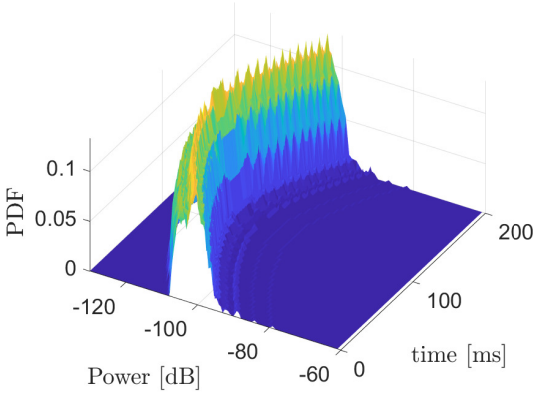

(a) PDF for the received power over time.

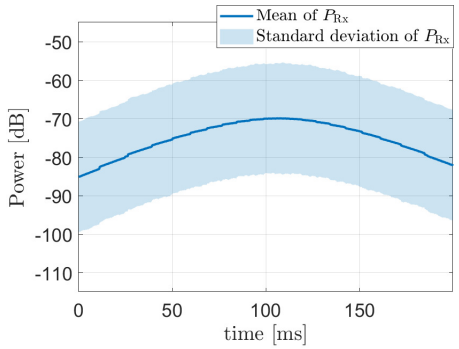

(b) Mean and standard deviation of the received power over time.

Fig. 6. Probabilistic description of received power levels.

IV. Results

In this Section, we numerically evaluate the received power with the displacement and rotation of the antenna using Eq. (10), and assuming the emitter power is $P_{\text{Tx}} = 30\,\text{dBm}$. To isolate the impact of the rotation speed, we consider the case where the receiver node flows in the center of the vessel and the transmitter moves on top at the distance of 2.5 times the shield's radius from the vessel center. In this setup, the transmitter is the only one rotating and at a very high frequency, as $\dot{\omega} \approx 692\,\text{rad/ms}$ indicated with Eq. (6).

We numerically evaluate the antenna's gain in the LoS link between both nanosensors; results are illustrated in Fig. 5. The transmitter gain oscillates due to the impact of rotation in

the antenna orientation. Although not rotating, the receiver also presents a time-varying gain due to the time-varying LoS direction with the emitter. Merging these two curves with the path loss component in Eq. (11) displays a receiver power that is also time-varying and largely impacted by the increasing distance between the emitter and the receiver.[5]

From this figure, we can also evaluate the impact of displacement and rotation. Comparing levels in Fig. 5, the antenna gain oscillates in the range -24 to $-12\,\mathrm{dBi}$, while the received power will be in larger amount, i.e, approximately in the range -90 to $-70\,\mathrm{dB}$. This is why we observe a remarked impact on the variability of the receiver power due to the antenna's rotation. Furthermore, in a practical scenario where the nanosensor's sensitivity is around the $-80\,\mathrm{dB}$, error-free communication can be conceived in a time window of around $100\,\mathrm{ms}$ (see the section where the blue line is above the dashed one in Fig. 5).

We also evaluate numerically the PDF for the received power with time. We simulate the mobility with initial random orientation angles as a combination of 30 different angles in the three axes for both antennas in the $[0,\, 2\pi]$ range. We record the received power level and numerically evaluate the PDF with the normalized histogram of the recorded power. As illustrated in Fig. 6a, the power level follows with the higher probability a close to a parabolic behavior with time; see Fig. 6b. The impact of distance mostly produces this behavior as the stronger attenuation component. Meanwhile, rotation is mostly producing variability around this peak value.

V. Conclusion

We presented a realistic simulation model to analyze the impact of nanoantenna mobility for in-body links. The simulator considers the realistic environment of human vessels, evaluating the impact of blood on the antenna radiation patterns and the mobility component. We observe that the displacement component introduces the mean value attenuation while the antenna's rotation mostly influences the variance around the mean. This study also provides the means to evaluate more metrics in the communication link. The channel coherence time and channel capacity can be further analyzed with the probabilistic description of the power level.

Acknowledgments

This work was supported in part by the project IoBNT funded by the German Federal Ministry of Education and Research (BMBF) under grant number 16KIS1986K and by the project NaBoCom funded by the German Research Foundation (DFG) under grant number DR 639/21-2.

References

[1] I. F. Akyildiz, F. Brunetti, and C. Blázquez, "Nanonetworks: A New Communication Paradigm," *Elsevier Computer Networks*, vol. 52, pp. 2260–2279, 2008.

[2] J. M. Jornet and A. Sangwan, "Nanonetworking in the Terahertz Band and Beyond," *IEEE Nanotechnology Magazine*, vol. 17, no. 3, pp. 21–31, Jun. 2023.

[5] See an animation of the nanosensor's mobility and the power levels in this video https://youtu.be/ADQ3YNwooLA

[3] J. M. Jornet and I. F. Akyildiz, "Graphene-based nano-antennas for electromagnetic nanocommunications in the terahertz band," in *EuCAP 2010*, Barcelona, Spain: EurAAP, Apr. 2010, pp. 1–5.

[4] M. Tamagnone, J. S. Gómez-Díaz, J. R. Mosig, and J. Perruisseau-Carrier, "Reconfigurable terahertz plasmonic antenna concept using a graphene stack," *Applied Physics Letters*, vol. 101, no. 21, Nov. 2012.

[5] S. Abadal, I. Llatser, A. Mestres, H. Lee, E. Alarcon, and A. Cabellos-Aparicio, "Time-Domain Analysis of Graphene-Based Miniaturized Antennas for Ultra-Short-Range Impulse Radio Communications," *IEEE Transactions on Communications*, vol. 63, no. 4, pp. 1470–1482, Apr. 2015.

[6] I. Llatser, C. Kremers, A. Cabellos-Aparicio, J. M. Jornet, E. Alarcón, and D. N. Chigrin, "Graphene-based nano-patch antenna for terahertz radiation," *Photonics and Nanostructures - Fundamentals and Applications*, vol. 10, no. 4, pp. 353–358, Oct. 2012.

[7] A. S. Thampy, M. S. Darak, and S. K. Dhamodharan, "Analysis of graphene based optically transparent patch antenna for terahertz communications," *Physica E: Low-dimensional Systems and Nanostructures*, vol. 66, pp. 67–73, Feb. 2015.

[8] H. Elayan, R. M. Shubair, J. M. Jornet, A. Kiourti, and R. Mittra, "Graphene-Based Spiral Nanoantenna for Intrabody Communication at Terahertz," in *IEEE AP-S/URSI 2018*, Boston, MA: IEEE, Jul. 2018.

[9] A. Abohmra, F. Jilani, H. T. Abbas, A. Alomainy, M. Ur-Rehman, M. A. Imran, and Q. H. Abbasi, "Flexible and Wearable Graphene-based Terahertz Antenna for Body-Centric Applications," in *IWMTS 2019*, Bad Neuenahr-Ahrweiler, Germany: IEEE, Jul. 2019.

[10] H. Gomez-Sousa, O. Rubinos-Lopez, and J. A. Martinez-Lorenzo, "Hematologic characterization and 3D imaging of red blood cells using a Compressive Nano-antenna and ML-FMA modeling," in *EuCAP 2016*, Davos, Switzerland: IEEE, Apr. 2016.

[11] S. Abadal, S. E. Hosseininejad, A. Cabellos-Aparicio, and E. Alarcon, "Graphene-Based terahertz antennas for area-constrained applications," in *TSP 2017*, Barcelona, Spain: IEEE, Jul. 2017.

[12] M. L. Scarpello, D. Kurup, H. Rogier, D. Vande Ginste, F. Axisa, J. Vanfleteren, W. Joseph, L. Martens, and G. Vermeeren, "Design of an Implantable Slot Dipole Conformal Flexible Antenna for Biomedical Applications," *IEEE Transactions on Antennas and Propagation*, vol. 59, no. 10, pp. 3556–3564, Oct. 2011.

[13] H. Elayan, R. M. Shubair, J. M. Jornet, and R. Mittra, "Multi-layer Intrabody Terahertz Wave Propagation Model for Nanobiosensing Applications," *Elsevier Nano Communication Networks*, vol. 14, pp. 9–15, Dec. 2017.

[14] J. T. Gómez, J. Simonjan, J. M. Jornet, and F. Dressler, "Optimizing terahertz communication between nanosensors in the human cardiovascular system and external gateways," *IEEE Communications Letters*, 2023.

[15] V. Jamali, A. Ahmadzadeh, W. Wicke, A. Noel, and R. Schober, "Channel Modeling for Diffusive Molecular Communication - A Tutorial Review," *Proceedings of the IEEE*, vol. 107, no. 7, pp. 1256–1301, Jul. 2019.

[16] N. Westerhof, F. Bosman, C. J. D. Vries, and A. Noordergraaf, "Analog studies of the human systemic arterial tree," *Journal of Biomechanics*, vol. 2, no. 2, pp. 121–143, May 1969.

[17] H. C. Berg, *Random Walks in Biology*. Princeton University Press, 1993.

[18] M. Fruchard, L. Arcese, and E. Courtial, "Estimation of the Blood Velocity for Nanorobotics," *IEEE Transactions on Robotics and Automation*, vol. 30, no. 1, pp. 93–102, Feb. 2014.

[19] S. Bridges and L. Robinson, *A Practical Handbook for Drilling Fluids Processing*. Elsevier, 2020.

[20] L.-H. Cai, T. E. Kodger, R. E. Guerra, A. F. Pegoraro, M. Rubinstein, and D. A. Weitz, "Soft Poly(dimethylsiloxane) Elastomers from Architecture-Driven Entanglement Free Design," *Advanced Materials*, vol. 27, no. 35, pp. 5132–5140, Aug. 2015.

[21] J. Happel and H. Brenner, *Low Reynolds number hydrodynamics: with special applications to particulate media* (Mechanics of Fluids and Transport Processes). Springer Dordrecht, 1983, p. 553.

[22] C. B. Reid, G. Reese, A. P. Gibson, and V. P. Wallace, "Terahertz Time-Domain Spectroscopy of Human Blood," *IEEE Journal of Biomedical and Health Informatics*, vol. 17, no. 4, pp. 774–778, Jul. 2013.

[23] J. Simonjan, B. D. Unluturk, and I. F. Akyildiz, "In-body Bionanosensor Localization for Anomaly Detection via Inertial Positioning and THz Backscattering Communication," *IEEE Transactions on NanoBioscience*, vol. 21, no. 2, pp. 216–225, Apr. 2022.